Research Square

Preprints are preliminary reports that have not undergone peer review.
They should not be considered conclusive, used to inform clinical practice,
or referenced by the media as validated information.

Towards Fire Digital Twin: Deep Learning Approach to Predicting Spatiotemporal Distribution of Fire Hazard Information

Zenghui Liu
Guanhua Qu
quguanhua93@126.com

Ming Yan
Lan Wang
Xin Liu
Gang Liu

Research Article

Keywords: Deep Learning, Sensor Performance, Cross-Physics Field, Evacuation Plane Monitoring, Fire Dynamics Simulation

Posted Date: March 9th, 2026

DOI: https://doi.org/10.21203/rs.3.rs-9046097/v1

License: This work is licensed under a Creative Commons Attribution 4.0 International License.
Read Full License

Additional Declarations: The authors declare no competing interests.

Version of Record: A version of this preprint was published at Fire Technology on May 25th, 2026. See the published version at https://doi.org/10.1007/s10694-026-01918-y.

Abstract

Accurately understanding the spatiotemporal distribution of key hazardous factors in fire scenes assists firefighters in making more informed decisions. This study developed a hybrid deep learning framework combining Long Short-Term Memory networks (LSTM) and Convolutional Neural Networks (CNN) to quickly identify fire source locations and incorporate fire source spatial information into the spatiotemporal prediction of hazardous factors. For fire source location identification, under a 1-second sampling interval, the average absolute error of the sensor's fire source coordinates was consistently below 0.1 meters. In the real-time monitoring of carbon monoxide, oxygen, and carbon dioxide, the CNN-LSTM model, after integrating non-temporal data such as fire source spatial information, significantly outperformed the baseline model in accuracy, achieving minimum normalized root mean square errors of 0.0333, 0.0402, and 0.0347, respectively. Moreover, in advance predictions up to 150 seconds before the fire scene, the model maintained extremely high levels of accuracy. Sensitivity analysis of sensor performance found that the accuracy of fire prediction can be attributed to the sampling interval, and compact time-series data can significantly improve prediction accuracy. This study has important practical significance for firefighters in formulating more reliable rescue plans.

1. Introduction

Building fires represent a lethal hazard that seriously threatens human life and property safety by generating high temperatures, smoke, and damaging building structures (Wang et al. 2022). In 2022, the United States reported approximately 1.5 million fire incidents, resulting in 3,790 deaths, 13,250 injuries, and property losses of about $18 billion (Hall and Evarts 2022). In the same year, China reported approximately 825,000 fire incidents, causing 2,053 deaths and 2,122 injuries (NFRA 2022).

Currently, research on fire scene situation detection using artificial intelligence is rapidly advancing (Khan et al. 2023; Liu et al. 2023c; Zeng et al. 2023). The earliest related studies focused on wildfire detection and fire risk assessment (Boroujeni et al. 2024; Khanmohammadi et al. 2024; McCracken et al. 2024; Moradi et al. 2024). Subsequently, some studies employed convolutional neural networks (CNNs) based on computer vision techniques for building fire detection (Hosseini et al. 2022; Khan et al. 2022; Majid et al. 2022; Feng and Sun 2024). By training fire test databases, numerical fire simulations, and fire smoke images (Hosseini et al. 2022; Khan et al. 2022; Majid et al. 2022; Wang et al. 2023b; Wang et al. 2023c; Feng and Sun 2024; Zhang et al. 2024a), artificial neural networks have been used to determine the fire heat release rate in real time (Wang et al. 2023b; Wang et al. 2023c), and attempts have been made to predict fire hazards such as flashovers (Zhang et al. 2024a).

Other studies have achieved significant results by expanding temperature sensor data. Kou developed a reverse model based on deep learning techniques, which can accurately identify the location and scale of fires in multiple compartments, achieving an accuracy of 92% on the test dataset (Kou et al. 2021). Shen, combining computational fluid dynamics (CFD) simulations with deep learning techniques, successfully realized the reverse tracking of fire source locations in single-room fires (Shen et al. 2023).

Wu's series of studies utilized long short-term memory (LSTM) deep learning models to identify real-time fire scenes and key fire events and proposed an intelligent fire digital twin system for monitoring and visualizing real-time 2D fire scenes (Wu et al. 2021; Wu et al. 2022).

However, existing studies primarily focus on certain fire characteristics, such as fire source location (Wu et al. 2021; Wu et al. 2022; Zhang et al. 2022b), heat release rate (Wang et al. 2023b; Wang et al. 2023c), and temperature fields (Wu et al. 2022; Zhang et al. 2022b), while research on real-time monitoring and prediction of other hazardous factors in fire scenes (e.g., CO, CO_2, O_2) remains relatively scarce. However, high-resolution and stable active information is required in widely used fields such as evacuation models (Li et al. 2023; Lyu et al. 2023; Wang et al. 2024c; Zhang et al. 2024b), fire search and rescue (Wu and Chen 2012; Lambert and Merci 2024), and robot-assisted firefighting (Sriniketh et al. 2023; Li et al. 2024; Zhao et al. 2024). Therefore, predicting the spatiotemporal distribution of fire scene hazardous factors with high resolution is crucial, as it can assist firefighters in making more accurate decisions and improve the reliability of their decisions (Junfeng et al. 2023).

Building fires are categorized into compartment fires and large-space fires, with current research mostly concentrated on compartment fires (Ji et al. 2024). Compartment fires are common in residential or office buildings, where hot gases fill the space over time, leading to flashovers and uniform temperature distribution (Kebriyaee et al. 2024; Helfenstein et al. 2025). In contrast, in large-space fires, hot air cannot fill the entire space, preventing flashovers and causing uneven temperature distribution. Moreover, the fire's location leads to variations in smoke distribution and production within the building's space (Liu et al. 2024). These differences in mechanisms highlight the necessity of studying large-space fires (Zhang et al. 2019). Furthermore, in smaller compartments, effective fire scene monitoring may be achievable using various point-type temperature and gas sensors. However, in large-space buildings, due to the large internal space, the effectiveness of automatic fire detection and suppression systems is limited (Chen and Guestrin 2016). Additionally, the trade-off between the cost of point sensors and the acquisition of high-resolution information remains a challenge (Qu et al. 2023).

In the face of these challenges, the advantages of expanding fiber optic temperature sensors to obtain multi-physical field information in fire scenes are becoming increasingly apparent. Fiber optic sensors offer several advantages, including long-distance measurement, continuous monitoring, resistance to electromagnetic interference, and corrosion resistance (Liu et al. 2023a). Liu constructed a dynamic calibration model through experimental research, enhancing the applicability of fiber optic sensors in high-temperature fire scenarios. Additionally, a data-driven method was adopted to achieve real-time mapping and future prediction of ceiling temperature fields for evacuation planes (Liu et al. 2023a; Liu et al. 2023b). Wang developed a cross-physical field mapping model based on the ANN algorithm, utilizing temperature field data from evacuation planes to output smoke field information (e.g., visibility, O_2, CO_2) (Wang et al. 2024a). Liu constructed a CO mapping model using random forests (Liu et al. 2024). These studies demonstrate that DTS provides abundant data sources, greatly promoting and expanding the application of artificial intelligence technologies in smart fire safety.

Compared to traditional machine learning algorithms, such as BP neural networks, long short-term memory (LSTM) networks offer significant advantages in processing temperature time-series data (Zhu et al. 2024). LSTM can capture long-term dependencies in time series and adapt to dynamic changes in data, while BP neural networks tend to suffer from gradient vanishing problems when handling long sequences (Hochreiter and Schmidhuber 1997; LeCun et al. 1998). Random forests and XGBoost are more limited in time-series data modeling, as they cannot fully leverage the temporal continuity of the data (Turska et al. 2021). The gating mechanism of LSTM enables more accurate predictions of temperature time-series data. Furthermore, CNN can explore the spatial features of the data, enhancing the accuracy of LSTM-based real-time predictions, such as fire monitoring applications (Zhang et al. 2022b).

In summary, this study aims to develop a spatiotemporal distribution prediction model for fire hazard factors in large building spaces based on the CNN-LSTM deep learning algorithm. The model's outputs include fire location, CO, CO_2, and O_2 concentrations at the 1.7-meter evacuation key plane. Furthermore, the model predicts the distribution of hazard factors at the 1.7-meter evacuation plane with lead times of 10s, 30s, 60s, 90s, 120s, and 150s. The structure of this paper is as follows: Section 2 introduces the model framework, including data acquisition, data processing, and model details; Section 3 presents the performance of the location prediction model; Section 4 evaluates the performance of the real-time monitoring and early prediction models; Section 5 discusses sensor parameters and presents the limitations and future directions of the research.

2. Methods

2.1 Research framework

The goal of this study is to use deep learning algorithms to monitor key fire information in large building spaces in real-time, including fire location, CO, CO_2, and O_2 concentrations at a 1.7m evacuation plane. Furthermore, the model predicts the distribution of hazard factors at the 1.7m evacuation plane for lead times of 10s, 30s, 60s, 90s, 120s, and 150s. Figure 1 illustrates the overall methodology and steps of this study: (1) Construction of a computational fluid dynamics (CFD) fire model, where virtual thermocouples are placed according to the layout strategy of the distributed fiber optic temperature sensor (DTS); (2) Data collection and processing, where different scanning window methods are employed to obtain sample sets from sensors with varying performances; (3) Selection of model hyperparameters based on prior knowledge and preliminary experiments; (4) Construction and training of the deep learning model.

2.2 Transient fire modeling

In an ideal scenario, it would be feasible to obtain sufficient sensor data from full-scale fire experiments or real fire events. However, the data available in the existing literature on large building fires is often insufficient and lacks systematic organization, which limits the potential application of deep learning. Therefore, a database constructed through large-scale numerical simulations can support the development of artificial intelligence-based fire prediction models. In this study, we employed the fire

dynamics simulation software FDS (version 6.7.6) for simulations. This software computes turbulence using large eddy simulation (LES) and direct numerical simulation (DNS) techniques (Liu et al. 2024), and its performance and accuracy have been widely recognized (Zhang et al. 2022b; Li et al. 2023; Shen et al. 2023). For the large building space in this study, the reliability of FDS was verified by full-scale experiments in the State Key Laboratory of Fire Science (Hefei, China)(Shan et al. 2025). Notably, our transient simulation is three-dimensional, whereas similar studies in the past have typically conducted two-dimensional simulations (Wu et al. 2021; Wu et al. 2022). Although three-dimensional simulations require more computational resources and time, they more realistically simulate the complex dynamics of fire spread, such as smoke behavior, heat transfer, and flame propagation paths, providing more accurate data support.

We selected a typical large-space model with dual-side exits for simulation. The space dimensions are 20m in length × 20m in width, with a total area of 400m². The ceiling plane is equipped with 400 thermocouples, and at the 1.7m evacuation plane, 400 gas-phase sensors for CO, CO_2, and O_2 are distributed, with sensor locations corresponding to the positions of the thermocouples. The simulation duration is 1000 seconds. In this study, we considered three parameters: fire location, fire intensity, and spatial height.

(1) **Fire Location**: The temperature variations and smoke distribution within a building are closely related to the location of the fire source (Wang et al. 2023a). During the development of a fire, hot smoke rises to form a smoke layer. The stability and flow characteristics of the smoke layer directly affect the temperature distribution in the lower layers. Different fire locations result in different positions and paths of the rising hot smoke, which in turn influences the formation and distribution of the smoke layer (Wang et al. 2023a). Therefore, accurately identifying the fire location can serve as an input for smoke prediction, enhancing the rationality and accuracy of the smoke prediction model. In this study, 16 fire locations were selected based on the spatial features of a typical model, as shown in Figure 1-step1.

(2) **Fire Intensity**: The t² model (Equation 1) is commonly used to describe the fire growth process and the variation of the heat release rate from the fire source over time. In the equation, Q represents the maximum heat release rate (kW), t is time (s), and a is the fire growth coefficient (kW/s²) (Hurley et al. 2015). According to the growth coefficient, the SFPE Handbook classifies fires into four types: slow fire, medium fire, fast fire, and ultra-fast fire (Hurley et al. 2015). Considering the different characteristics of fire development, this study selects medium fire, fast fire, and ultra-fast fire as the three types for scenario construction, with corresponding aa values of 0.01172 kW/s², 0.0469 kW/s², and 0.1876 kW/s², respectively. According to DGJ08-88-2006, the maximum heat release rate, Q, is set to 20 MW, and the times to reach the maximum heat release rate at different heating rates are 326.5s, 653s, and 1306.3s, respectively.

$$Q=at^2 \qquad (1)$$

(3) **Spatial Height**: Spatial height has a significant impact on temperature and smoke distribution in large building fires. In high spaces, heat and smoke tend to rise and accumulate at higher positions, forming a

smoke layer, which may cause the temperature in lower regions to be relatively lower, affecting fire detection and response strategies. In contrast, in low spaces, smoke has a higher likelihood of coming into contact with humans, concentrating heat and increasing the heat release rate and smoke concentration, thereby making evacuation and rescue more difficult. This study selects 4m, 6m, and 9m as the variables for spatial height (Liu et al. 2024).

During the simulation process, to achieve accurate smoke flow prediction, it is typically recommended that the model grid size be between 1/4 and 1/16 of the characteristic fire source diameter (Baker et al. 2020). Given that the characteristic diameter of a typical fire source is 1.80 meters, we selected grid sizes of 0.125 meters, 0.25 meters, and 0.45 meters (Wang et al. 2024a). By analyzing the temperature at the fire evacuation plane (z = 1.7m), the results showed that when a 0.25-meter grid size was used, the average temperature over the entire FDS simulation had mean absolute percentage errors (MAPE) of 0.82% and 3.71% compared to the 0.125-meter and 0.45-meter grid sizes, respectively. Since the average deviation for the 0.25-meter grid size was less than 1% compared to the 0.125-meter grid, it can be concluded that the 0.25-meter grid size meets the grid independence requirements for the simulation calculations.

2.3 Database Construction

To construct a training database suitable for deep learning algorithms, the simulation results were systematically organized and processed. Figure 1-Step2 illustrates the process of database generation in detail. The database includes temperature data measured by thermocouples, gas concentration data, and fire scenario information. In practical applications, the temperature data from 400 thermocouples is provided by the DTS and serves as the sole sensor input in our operational process. To evaluate the performance of different sensor characteristics (i.e., the sensor sampling interval or data refresh rate) in predicting fire field information using deep learning models, we employed a window scanning sample generation method. By adjusting the window size and sampling interval, 36 different input combinations were generated, where the sampling intervals (SI) included 1, 3, 5, and 10 seconds, and the time lengths (TL) included 20, 30, 40, 50, 60, 70, 80, 90, and 100 seconds. It is important to note that TL refers to the period from the first data point to the last data point within the sample, rather than the number of data points. For example, when SI = 3 seconds and TL = 60 seconds, the sample contains 20 data points. The data were then labeled, with output variables including the fire location and the concentrations of CO, CO_2, and O_2 at the evacuation plane. Finally, the data underwent standardization, shuffling, and splitting. Standardization of inputs and outputs is crucial for facilitating the training process and enhancing model performance. In this study, the Standard Scaler was used to scale all input and output data, after which the samples were randomly shuffled using the “shuffle” method. The database samples were then split into a training set and a test set at an 8:2 ratio.

2.4 Deep learning model for fire prediction

2.4.1 Input and output of the model

After the database construction is completed, as shown in Figure 2-Agent I, the inverse fire location identification model can directly input the database and output the horizontal and vertical coordinates of the fire location on the plane. However, for the forward prediction model of the spatiotemporal distribution of fire hazards, the input data require further processing. This study aims to map the smoke distribution data on the evacuation plane using ceiling temperature data, as shown in Figure 2-Agent II. Specifically, for each target point, the model's input includes the temperature data selected from 9 temperature sensors vertically above the 400 temperature measurement points. Additionally, four parameters are included: space height (SH), the distance from the fire source to the nearest opening (d_{open}), the distance from the fire source to the nearest wall (d_{wall}), and the distance from the target point to the fire source (d_{fire}). The model's output consists of the real-time and different lead-time (PT = 10s, 30s, 60s, 90s, 120s, 150s) concentration distributions of CO, CO_2, and O_2 on the evacuation plane.

2.4.2 Deep learning model structure

In this study, the inverse fire location identification model employs the Long Short-Term Memory (LSTM) algorithm (Hochreiter and Schmidhuber 1997). LSTM is a specialized type of Recurrent Neural Network (RNN) designed for sequence data, capable of passing information through hidden states. Traditional RNNs suffer from gradient vanishing problems (Su et al. 2018), but LSTM incorporates gating mechanisms—including input, forget, and output gates—that effectively control the storage, updating, and output of information. This architecture allows LSTM to capture long-term dependencies and address the gradient vanishing issue (Su et al. 2018). As shown in Figure 2-Agent I, the inverse fire location identification model consists of two LSTM layers, each with 100 states, followed by a fully connected Dense layer with 50 states and a ReLU activation function, and a final output layer with 2 states and a linear activation function.

For the forward prediction model of fire hazard factors' spatiotemporal distribution, this study employs a CNN-LSTM hybrid model. CNN-LSTM is specifically designed to address data problems that involve both spatial features and temporal sequences (Fahim et al. 2025). In this architecture, the CNN component processes the input data to extract spatial features, which are then passed to the LSTM component to capture the temporal dependencies. As shown in Figure 2-Agent II, the time-series data part of the model consists of two convolution layers, two pooling layers, and two LSTM layers, while the non-time-series data is processed by a fully connected layer. The outputs from both parts are merged through a concatenation layer and input into two fully connected layers.

During the model construction, initial choices were made for different activation functions, loss functions, optimizers, dropout rates, and regularization coefficients (L1 and L2) based on prior knowledge (see Figure 1-Step3). Initial validation showed that the ReLU activation function converged significantly faster than tanh and sigmoid, while the Adam optimizer outperformed RMSprop (see Appendix A1-a). Other hyperparameters were selected as follows: Mean Squared Error (MSE) as the loss function, dropout rate of 0, L1 regularization coefficient of 0, and L2 regularization coefficient of 0.001

(see Appendix A1-b). The model batch size was set to 200, with 500 epochs for training. All models were trained three times, and the final metrics were averaged.

2.4.3 Evaluation indicators

In evaluating the performance of machine learning models, common metrics include Mean Squared Error (MSE), Root Mean Squared Error (RMSE), Mean Absolute Error (MAE), Mean Absolute Percentage Error (MAPE), and R-squared (R^2), among others. These metrics assess the model's prediction accuracy and stability from different perspectives (Liu and Lin 2024; Liu and Zhuang 2024; Fahim et al. 2025). However, since different datasets may have varying units and scales, directly comparing model performance using these metrics could lead to results lacking comparability. To overcome this limitation, this study introduces the Normalized Root Mean Squared Error (NRMSE) as a dimensionless evaluation metric (Sangogboye et al. 2017; Niu et al. 2018). NRMSE standardizes RMSE, eliminating the influence of the original data scale, thus enabling unified evaluation across datasets with different scales. By combining MSE, RMSE, MAE, MAPE, R^2, and NRMSE, this study provides a more accurate reflection of machine learning models' performance in complex applications like fire prediction, ensuring the comprehensiveness and scientific validity of the evaluation results, and thus enhancing the model's effectiveness and reliability in real-world applications.

3. Fire source location identification

Accurate prediction of fire location in advance is crucial to mitigate the potentially severe consequences of a fire. Table 1 presents the test set results for 36 scenarios with four different sensor time sampling intervals and nine different time lengths. For the nine scenarios with a sampling interval (SI) of 1 second, the average absolute error (MAE) of the fire source center’s x and y coordinates was less than 0.1 meters across all time lengths, with the average absolute percentage error (MAPE) remaining below 3%. Specifically, for a time length (TL) of 80 seconds, the MAE was at its lowest, below 0.03 meters, and the MAPE was under 1%. For the nine scenarios with an SI of 3 seconds, although the MAE reached its lowest point at TL=100 seconds, the model still demonstrated good performance across the TL range of 20 seconds to 90 seconds. Except for TL=20 seconds, the R^2 value for all other models was above 0.9. For the nine scenarios with an SI of 5 seconds, the prediction performance significantly dropped for the TL=20 seconds scenario, with MAE values of 1.4171 meters for the x coordinate and 1.5976 meters for the y coordinate. For the SI=10 seconds scenarios, the R^2 value of the model reached 0.9 only at TL=90 seconds.

In conclusion, this study found that when the sampling intervals were 1 second, 3 seconds, and 5 seconds, the fire location recognition model achieved an R^2 value close to 0.9 with a threshold of TL=30 seconds. Compared to Fang et al.’s reverse prediction of fire location in a single room, the minimum MAPE for the x and y coordinates in this study were 0.87% and 0.86%, significantly outperforming their values of 8.9% and 3% (Fang et al. 2023). This improvement is mainly attributed to the use of a deep

learning method based on LSTM in this study, which effectively leveraged the complex relationships within temperature time series, enhancing prediction accuracy.

Furthermore, to better illustrate the model's performance in fire location recognition, as shown in Figure 3-a, we selected one-quarter of the original study area and used 16 different colors to represent 16 initial fire locations, displaying the fire location recognition results for the test set under 20 different sensor scenarios. It can be observed from the figure that, with the increase in time length, the recognition scatter points for all sensor intervals gradually converge. This suggests that longer monitoring periods help improve the accuracy of fire location recognition. Additionally, with the increase in sensor interval, the variation patterns of the recognition results differ, possibly due to the reduction in sensor data acquisition frequency, which affects the ability to respond promptly to dynamic fire changes.

Furthermore, by examining the trend of the average absolute error (MAE) of the x and y coordinates predicted for the test set under four SI conditions as the time length (TL) increases (Figures 3-b and 3-c), the results show that for any SI, as TL increases, the rate of decrease in MAE gradually slows down. This indicates that after reaching a certain "saturation point," the marginal benefit of increasing the number of data points declines. This suggests that, in practical applications, although extending the monitoring time may slightly improve prediction accuracy, it is more reasonable to select an appropriate time length to achieve efficient prediction when resources are limited.

Table 1 Results of fire source location identification

SI	TL	X-axis				Y-axis			
		MAE	RMSE	MAPE	R^2	MAE	RMSE	MAPE	R^2
1s	20s	0.0801	0.1757	0.0294	0.9972	0.0800	0.1784	0.0292	0.9970
	30s	0.0572	0.1172	0.0198	0.9988	0.0600	0.1015	0.0225	0.9991
	40s	0.0404	0.1162	0.0151	0.9986	0.0382	0.0759	0.0136	0.9995
	50s	0.0404	0.0667	0.0149	0.9996	0.0420	0.0712	0.0157	0.9994
	60s	0.0339	0.0526	0.0122	0.9997	0.0334	0.0713	0.0120	0.9995
	70s	0.0420	0.0736	0.0148	0.9992	0.0419	0.0623	0.0150	0.9995
	80s	**0.0238**	**0.0421**	**0.0087**	**0.9998**	**0.0236**	**0.0382**	**0.0086**	**0.9998**
	90s	0.0269	0.0425	0.0093	0.9998	0.0281	0.0421	0.0108	0.9998
	100s	0.0348	0.0493	0.0121	0.9996	0.0432	0.0841	0.0160	0.9991
3s	20s	0.7224	1.1233	0.2697	0.8916	0.6801	1.0650	0.2375	0.8991
	30s	0.2814	0.4896	0.1031	0.9794	0.2981	0.5249	0.1121	0.9754
	40s	0.1945	0.4271	0.0689	0.9830	0.1867	0.4276	0.0702	0.9833
	50s	0.1654	0.3764	0.0750	0.9874	0.1540	0.2793	0.0498	0.9931
	60s	0.1707	0.3518	0.0700	0.9889	0.1673	0.2823	0.0608	0.9930
	70s	0.1287	0.2489	0.0486	0.9942	0.1193	0.2028	0.0463	0.9963
	80s	0.1014	0.1795	0.0343	0.9970	0.1066	0.1718	0.0361	0.9973
	90s	0.0958	0.2016	0.0326	0.9965	0.1127	0.2416	0.0370	0.9947
	100s	**0.0553**	**0.1129**	**0.0192**	**0.9989**	**0.0560**	**0.0850**	**0.0196**	**0.9994**
5s	20s	1.4171	1.9303	0.5500	0.6643	1.5976	2.1583	0.7072	0.6075
	30s	0.7629	1.1221	0.3132	0.8918	0.7982	1.1491	0.3172	0.8806
	40s	0.6188	1.0463	0.2462	0.9037	0.5783	0.9204	0.2390	0.9240
	50s	0.4227	0.6657	0.1425	0.9598	0.3994	0.6366	0.1736	0.9645
	60s	0.4596	0.7776	0.1792	0.9338	0.4864	0.7582	0.1735	0.9340
	70s	0.2490	0.4242	0.0954	0.9835	0.2684	0.4231	0.0968	0.9829
	80s	0.2268	0.3809	0.0881	0.9872	0.2255	0.3650	0.0790	0.9885
	90s	0.2029	0.3598	0.0914	0.9886	0.1979	0.3168	0.0685	0.9912
	100s	**0.1702**	**0.2728**	**0.0651**	**0.9935**	**0.1795**	**0.2839**	**0.0648**	**0.9929**

10s	20s	2.6119	3.1340	1.3108	0.1799	2.6488	3.1806	1.2487	0.1172
	30s	2.2582	2.8089	0.9990	0.2762	2.1957	2.7386	0.8459	0.2960
	40s	1.7561	2.3837	0.7106	0.5211	1.7581	2.3303	0.7271	0.5379
	50s	1.3769	1.9320	0.5770	0.6884	1.4227	1.9469	0.5083	0.6680
	60s	1.0558	1.5539	0.4035	0.7853	1.0233	1.4705	0.4156	0.8092
	70s	0.8245	1.2165	0.3063	0.8686	0.8356	1.2467	0.3349	0.8562
	80s	0.7420	1.1259	0.2862	0.8897	0.7591	1.1910	0.3201	0.8757
	90s	**0.5504**	**0.8191**	**0.2039**	**0.9407**	0.5992	0.9185	0.2505	0.9245
	100s	0.5313	0.9123	0.2413	0.9318	**0.5018**	**0.7459**	**0.1722**	**0.9493**

4. Prediction of spatiotemporal distribution of risk factors

4.1 Evaluation of prediction results

In evaluating the spatiotemporal distribution prediction model for fire hazard factors, we obtained a rich dataset from transient numerical simulations of fire scenarios lasting up to 1000 seconds (with an average of 18 hours of computation on an I9-13980hx processor with 32GB of RAM). The maximum concentration of carbon monoxide (CO) reached 4005 ppm, with 45% of CO data below 120 ppm, and the data skewness was 0.919, showing a right-skewed distribution. The maximum concentration of carbon dioxide (CO_2) reached 100,000 ppm, also showing a right-skewed distribution, while oxygen (O_2) data exhibited a left-skewed distribution. These data characteristics suggest significant differences in the numerical range and distribution shape of the collected gas concentration data, adding complexity to the model evaluation.

Given the wide range of the dataset, we selected multiple evaluation metrics to comprehensively assess the model's performance, including MAE, RMSE, R^2, and the dimensionless metric NRMSE. NRMSE standardizes the RMSE, eliminating the impact of differing units and scales on model evaluation, and enabling consistent comparison across datasets. Additionally, to compare with existing research results, we selected the Random Forest model, which has demonstrated optimal performance in real-time monitoring in the relevant literature, and trained our dataset following the same data processing methods as previous studies. This model served as the baseline (Base model) to provide a reference for evaluating the real-time monitoring model proposed in this study. By comparing with the baseline model, we can more clearly demonstrate the advantages and improvements of the proposed model across different evaluation metrics, thereby verifying its effectiveness and superiority.

4.2 Spatiotemporal distribution prediction of CO distribution

Monitoring and obtaining the concentration of carbon monoxide (CO) during a fire is crucial (Sriniketh et al. 2023; Wang et al. 2024b). CO is a colorless, odorless, and highly toxic gas that rapidly binds with

hemoglobin, hindering oxygen transport and leading to suffocation and poisoning. During the development of a fire, hot smoke rises and forms a smoke layer, and the stability and flow characteristics of this layer directly affect the temperature distribution in the lower layers. The position of the fire determines where and how the hot smoke rises, thus influencing the formation and distribution of the smoke layer. Real-time monitoring of CO concentration can help detect the accumulation of toxic gases in a fire, enabling timely emergency evacuation and rescue measures to reduce the risk of poisoning and death. Moreover, changes in CO concentration can serve as an important indicator for evaluating the fire development stages and the intensity of the fire source, aiding firefighters in formulating more scientific and effective firefighting strategies.

Figures 4-a and 4-b show the trends of the normalized root mean square error (NRMSE) and mean absolute error (MAE) of the CO real-time monitoring model as the time length (TL) increases under four different sampling interval (SI) conditions. The gray line represents the baseline model's prediction results. As can be seen, except for the sensor scenarios with SI = 10 seconds and TL = 20 seconds and 30 seconds, the deep learning model based on the CNN-LSTM algorithm proposed in this study outperforms all other scenarios in terms of prediction accuracy. The minimum MAE for the deep learning model is 68 ppm (SI = 1s, TL = 40s), and the minimum NRMSE is 0.0333 (SI = 1s, TL = 70s). Further, eight sensor performance scenarios with SI = 1 second and TL = 20 seconds were selected, and the comparison between the true values and predicted values of the test set is shown in Figure 4c. The density plot shows that CO data mainly concentrates in the range of 0-500 ppm, and the model achieves excellent prediction accuracy (MAE = 12.07 ppm) within this concentration range.

In this study, a matrix bubble comparison chart was used to display the MAE results of CO prediction 10s to 150s in advance under different sampling intervals (SI = 1s, 3s, 5s) (Figure 5-a). The x-axis of each chart represents the forecasted lead time (20s to 100s), and the y-axis represents the prediction time (30s to 150s). The size of the bubbles represents the MAE value, with larger bubbles indicating higher prediction errors. From the results, it can be observed that as the forecast lead time increases, the MAE generally shows an upward trend, especially for longer prediction time periods (such as the 90s to 120s), indicating that prediction accuracy decreases with longer forecast lead times. Furthermore, the sampling interval has a significant impact on the prediction error. For example, under SI = 1s, the prediction error is relatively low, while under SI = 5s, the prediction error is higher. This could be related to the reduction in data sampling frequency, which results in information loss. Additionally, we selected four representative measurement points under different heights and fire source conditions to demonstrate the accuracy of our model (Figures 5-b, 5-c, and 5-d). The results show that the model has high prediction accuracy for CO growth curves, regardless of whether a plateau phase exists, and for different value ranges (for example, in some conditions, CO concentration peaks can reach up to 4000 ppm).

Fig 4 shows the results of the CO real-time monitoring model: (a) NRMSE as it changes with TL under four different SI conditions, (b) MAE as it changes with TL under four different SI conditions, and (c) the comparison between the true values and predicted values for eight cases.

Fig 5 shows the results of the CO advanced monitoring model: (a) MAE as it changes with TL and PT under four different SI conditions, (b) comparison of predictions for four representative measurement points in a medium-speed fire scenario with a source location at (1m, 1m) and a height of 4m, (c) comparison of predictions for four representative measurement points in a fast fire scenario with a source location at (1m, 10m) and a height of 6m, and (d) comparison of predictions for four representative measurement points in an ultra-fast fire scenario with a source location at (10m, 1m) and a height of 9m.

4.3 Spatiotemporal distribution prediction of O_2 distribution

The measurement of oxygen (O_2) concentration plays a crucial role in fire warning and control. As a necessary condition for fire combustion, a decrease in oxygen concentration directly affects the combustion rate of the fire and its ability to spread (Zhang et al. 2022a). By real-time monitoring of O_2 concentration, potential dangers in the fire can be detected early, enabling rapid isolation and control measures to suppress the spread of the fire. In addition, changes in O_2 concentration can help assess the ventilation conditions of the fire scene and the oxygen supply in the space, thereby optimizing the design and operation of fire prevention and control systems to ensure that the fire source can be effectively controlled during the fire, minimizing the damage caused by the fire.

Figures 6-a and 6-b show the trends of the normalized root mean square error (NRMSE) and mean absolute error (MAE) for the O_2 real-time monitoring model as the time length (TL) increases under four different sampling interval (SI) conditions. The gray line represents the prediction results of the baseline model. In the SI = 1 second and SI = 3 seconds sensor scenarios, the model performance is better than that of the baseline model. However, when SI = 5 seconds, the model's accuracy is lower than that of the baseline model at TL = 20 seconds, but it becomes comparable to the baseline model between TL = 30 seconds and TL = 50 seconds. Beyond TL = 50 seconds, the model's performance drops again, falling below the baseline model's performance. Compared with the CO real-time monitoring model, the advantages of the deep learning model are somewhat reduced, but it still maintains an edge within a relatively large range. The minimum MAE for the deep learning model is 0.0033, and the NRMSE is 0.0402 (SI = 1s, TL = 40s). Figure 6-c shows the comparison between the true values and predicted values for the test set under eight sensor performance scenarios, such as SI = 1s and TL = 20s. From the density plot, it can be seen that the oxygen data mainly concentrates in the range of 0.18 to 0.2, and the model demonstrates excellent prediction accuracy within this concentration range.

For the early prediction model of O_2, as shown in Figure 7-a, the MAE range under different sampling intervals is between 0.0036 and 0.0080. Similar to the CO prediction results, regardless of whether the sampling interval is 1 second, 3 seconds, or 5 seconds, the MAE gradually increases as the forecast lead time increases. This trend suggests that over longer forecast periods, the prediction error accumulates, resulting in reduced prediction accuracy. For smaller sampling intervals (such as SI = 1s), the model’s performance improvement is not significant when the prediction lead time (TL) is extended. This may be

because short-term predictions already provide relatively accurate results, and increasing the sampling frequency has a limited impact on improving the MAE.

Further analysis of Figures 7-b, 7-c, and 7-d reveals that the O_2 early prediction model successfully tracks O_2 curves with different decreasing trends under various fire scenarios. This indicates that regardless of how the rate of decrease in oxygen concentration changes in the fire scene, the model can effectively capture its pattern. This characteristic demonstrates the model's excellent generalization ability when faced with different fire scenarios, allowing it to adapt to various environmental conditions and make accurate predictions. Additionally, from these charts, it can be observed that despite the differences in sampling intervals and prediction times, the model still performs well in predicting the changes in oxygen concentration in the fire scene, proving the reliability and adaptability of the model in practical applications.

Fig 6 shows the results of the O_2 real-time monitoring model: (a) NRMSE as it changes with TL under four different SI conditions, (b) MAE as it changes with TL under four different SI conditions, and (c) the comparison between the true values and predicted values for eight cases.

Fig 7 shows the results of the O_2 advanced monitoring model: (a) MAE as it changes with TL and PT under four different SI conditions, (b) comparison of predictions for four representative measurement points in a medium-speed fire scenario with a source location at (1m, 1m) and a height of 4m, (c) comparison of predictions for four representative measurement points in a fast fire scenario with a source location at (1m, 10m) and a height of 6m, and (d) comparison of predictions for four representative measurement points in an ultra-fast fire scenario with a source location at (10m, 1m) and a height of 9m.

4.4 Spatiotemporal distribution prediction of CO_2 distribution

The monitoring of carbon dioxide (CO_2) concentration also plays a crucial role in fire management. CO_2 is one of the primary gases produced during fire combustion, and its concentration increase not only reflects the intensity and scale of the fire but also affects the indoor air quality and the respiratory conditions of individuals. By monitoring CO_2 concentration, it is possible to determine whether the fire is worsening, adjust ventilation and firefighting measures promptly, and prevent the spread of the fire and the accumulation of smoke. Furthermore, changes in CO_2 concentration can assist in evaluating the combustion efficiency and fuel type of the fire, providing valuable data support for post-fire damage assessment and recovery efforts.

Figures 8-a and 8-b show the trends of the normalized root mean square error (NRMSE) and mean absolute error (MAE) for the CO_2 real-time monitoring model as the time length (TL) increases under four different sampling interval (SI) conditions. The gray line represents the prediction results of the baseline model. The results indicate that the prediction performance for most sensor scenarios is still better than that of the baseline model, with the deep learning model achieving a minimum NRMSE of 0.0364 (SI =

1s, TL = 40s). Figure 8-c shows the comparison between the true values and predicted values for the test set under eight sensor performance scenarios, such as SI = 1s and TL = 20s.

For the CO_2 early prediction model, it can be observed that as the forecast lead time increases, the MAE gradually increases. However, compared with the CO and O_2 models, the MAE difference between the longer and shorter forecast lead times is greater for the CO_2 model. For example, at SI = 1s and TL = 20s, the MAE at a 150s lead time is 71.50% higher than at a 10s lead time. This data contrasts with the CO and O_2 models, which show MAE increases of 34.79% and 64.86%, respectively. This suggests that the CO_2 model requires temperature data with a smaller SI to achieve better results, meaning sensors with better data refresh performance are needed.

Fig 8 shows the results of the CO_2 real-time monitoring model: (a) NRMSE as it changes with TL under four different SI conditions, (b) MAE as it changes with TL under four different SI conditions, and (c) the comparison between the true values and predicted values for eight cases.

Fig 9 shows the results of the CO_2 advanced monitoring model: (a) MAE as it changes with TL and PT under four different SI conditions, (b) comparison of predictions for four representative measurement points in a medium-speed fire scenario with a source location at (1m, 1m) and a height of 4m, (c) comparison of predictions for four representative measurement points in a fast fire scenario with a source location at (1m, 10m) and a height of 6m, and (d) comparison of predictions for four representative measurement points in an ultra-fast fire scenario with a source location at (10m, 1m) and a height of 9m.

5. Discussion

5.1 Sensor performance discussion

In complex and urgent fire scenarios, time efficiency is crucial. Due to resource limitations or specific application needs, the sampling interval of sensors may need to be appropriately adjusted. Therefore, to achieve the optimal balance between prediction accuracy and response efficiency and ensure effective fire emergency management, it is necessary to discuss sensor performance in detail.

Figure 10-a shows the trend of average MAE as the number of temperature points increases under four different SI conditions. Overall, prediction accuracy relies more on the number of collected temperature points than on the time sampling interval (SI). However, within a limited data collection period (as it is impractical to spend too much time making judgments during an actual fire), the impact of data quantity is essentially equivalent to the sampling interval (SI). This finding is consistent with the conclusions of Wu et al. who used artificial intelligence and numerical databases to build a tunnel fire prediction model (Wu et al. 2021). Although, overall, prediction accuracy can be attributed to the number of collected temperature points, we observe that in the three scenarios of "SI=1, TL=20", "SI=3, TL=60", and "SI=5, TL=100" where the number of temperature points is 20, the accuracy is close but still shows some differences. The corresponding average MAEs are 0.08m, 0.169m, and 0.1749m. This gap is further

expanded in the scenarios with 10 temperature points, specifically "SI=3, TL=30", "SI=5, TL=50", and "SI=10, TL=100", with the corresponding average MAEs being 0.2898m, 0.4111m, and 0.5166m. This demonstrates that compact time-series data is superior to sparse temperature sensor data for location prediction models.

Figure 10-b shows the trend of MAE for the three hazardous factor monitoring models as the number of temperature points increases. Compared to the location model, the curves for the hazardous factor models fluctuate more, exhibiting some consistency in fluctuation. However, we can still generally say that prediction accuracy can be attributed to the number of collected temperature points. Further analysis shows that the inflection point of the curves occurs around 10, and as the number of temperature data points exceeds 10, the model's accuracy begins to fluctuate. These data indicate that increasing the number of temperature points and using shorter sampling intervals can significantly improve the accuracy of hazard monitoring models. However, once the "performance saturation point" is reached, the marginal benefits of increasing the number of temperature points disappear (Liu et al. 2024). This is crucial for improving prediction capabilities and enhancing model effectiveness.

In practical applications, lower sampling intervals can provide more timely and accurate fire location predictions, aiding in rapid response and effective evacuation. Additionally, although higher sampling intervals may reduce the burden on data processing and transmission, this requires a trade-off between system resources and response speed. Considering the above factors, this study recommends prioritizing sensors with an SI of 1 second or 3 seconds in fire monitoring systems to ensure that the fire source can be located promptly and accurately in emergencies, minimizing the potential risks and losses caused by fire. Future research can further explore the impact of different sensor layouts and additional sensor data types on the performance of fire location prediction models to achieve a more comprehensive and robust fire monitoring solution.

Fig 10 shows the change in model performance with the number of temperature points: (a) Location prediction model, (b) Hazard factor spatiotemporal prediction model.

5.2 Limitations and Prospects

This paper proposes a method to help firefighters in real-time identification of the spatiotemporal distribution of fire hazards in large space buildings, which will provide significant support for building fire rescue and evacuation. However, existing research has some limitations: first, the current training database is built using a limited number of simplified fire scenarios, and it should include more realistic fire scenarios for future AI model training. Additionally, although the trained agent performs well on most test data samples, larger errors may still occur in certain samples. To improve the model's reliability, physical constraints describing fire evolution laws will be incorporated into the training process to ensure the rationality of the model's output.

To enhance the model's generalization and achieve highly intelligent firefighting engineering, future work will focus on the following areas: first, future research will focus on increasing the realism of fire

modeling. The shape of spaces, ventilation systems, and blockages can significantly affect temperature distribution and smoke movement, so more fire scenarios need to be modeled. This will further expand the model's consideration of the impact of varying maximum heat release rates under different fire growth conditions. Secondly, adequate real-time experimental validation is crucial for the practical application of machine learning models. Furthermore, more real fire tests will be conducted to collect data, supporting the optimization of the model.

6. Conclusion

This study proposes a deep learning framework that includes LSTM and CNN for identifying fire source locations in large building spaces. It uses fire source spatial information as non-temporal data along with temperature time-series data as inputs to build a spatial-temporal prediction model for fire hazard factors. The model can output high-resolution maps of CO, O_2, and CO_2 in real-time, as well as for time-lags of 10s, 30s, 60s, 90s, 120s, and 150s in advance. The specific conclusions are as follows:

（1）The model performs excellently in fire location prediction, with MAE of sensor fire source coordinates under a 1-second sampling interval all below 0.1 meters. The MAPE of the x, y coordinates with the 30s of input data are 1.98% and 2.25%, and the minimum MAPE values are 0.86% and 0.86% (TL=80s), significantly outperforming the traditional BP neural network's prediction accuracy (8.9% and 3%).

（2）For real-time monitoring of CO, O_2, and CO_2, the CNN-LSTM model, by incorporating non-temporal data such as fire source spatial information, achieves accuracy far beyond the baseline model (RF), with minimum NRMSE values of 0.0333, 0.0402, and 0.0347, respectively. For the advanced prediction of CO, O_2, and CO_2, the model exhibits excellent performance across prediction horizons from 10s to 150s and can recognize different trends in smoke variation.

（3）A sensitivity analysis of sensor performance shows that the accuracy of fire location prediction primarily depends on the number of temperature data points rather than the sampling interval (SI). However, within a limited data collection period, the impact of data quantity is essentially equivalent to that of SI. Additionally, compact time-series data significantly improves prediction accuracy. For the same number of data points, shorter sampling intervals (e.g., 1s or 3s) outperform longer sampling intervals (e.g., 5s or 10s) in terms of performance.

This work confirms the feasibility of using deep learning to extend temperature data for cross-physical field prediction of spatial-temporal distributions of key evacuation parameters, such as carbon monoxide, in large building fire environments. The research conclusions will have significant positive implications for the planning of escape routes for evacuees and the arrangement of rescue plans for firefighters, and they lay the foundation for future emergency response strategies in smart cities.

Declarations

Acknowledgments

The authors would like to thank the research participants for assisting in this study. This study was supported by the Multiple investment in applied basic research of Tianjin (Urban Fire Protection Project - Grant No. 22JCYBJC01710, No.22JCZDJC00850) This research is financially supported by the National Natural Science Foundation of China (No.52378174) and Tianjin University Engineering Master Innovation practice project.

References

1. Baker N, Kelly G, O'Sullivan PD (2020). A grid convergence index study of mesh style effect on the accuracy of the numerical results for an indoor airflow profile. International Journal of Ventilation, 19: 300-314.
2. Boroujeni SPH, Razi A, Khoshdel S, et al. (2024). A comprehensive survey of research towards AI-enabled unmanned aerial systems in pre-, active-, and post-wildfire management. Information Fusion, 108: 102369.
3. Chen T, Guestrin C (2016). Xgboost: A scalable tree boosting system. Proceedings of the 22nd acm sigkdd international conference on knowledge discovery and data mining. 785-794.
4. Fahim BM, Akbar MK, Amayri M (2025). ResiDualNet: A novel electric vehicle charging data imputation technique to enhance load forecasting accuracy. Building Simulation.
5. Fang H, Xu M, Zhang B, et al. (2023). Enabling fire source localization in building fire emergencies with a machine learning-based inverse modeling approach. Journal of Building Engineering, 78: 107605.
6. Feng J, Sun Y (2024). Multiscale network based on feature fusion for fire disaster detection in complex scenes. Expert Systems with Applications, 240: 122494.
7. Hall S, Evarts B (2022). Fire loss in the United States during 2021. National Fire Protection Association (NFPA).
8. Helfenstein RP, Lemmertz CK, Centeno FR (2025). The impact of fire source location on hot gas layer temperature in multi-compartment pre-flashover fires: Analysis and semi-empirical model development. International Journal of Thermal Sciences, 208: 109464.
9. Hochreiter S, Schmidhuber J (1997). Long Short-Term Memory. Neural Computation, 9: 1735-1780.
10. Hosseini A, Hashemzadeh M, Farajzadeh N (2022). UFS-Net: A unified flame and smoke detection method for early detection of fire in video surveillance applications using CNNs. Journal of Computational Science, 61: 101638.
11. Hurley MJ, Gottuk DT, Hall Jr JR, et al. (2015). SFPE handbook of fire protection engineering. Springer.
12. Ji W, Li G-Q, Zhu S, et al. (2024). Machine learning-driven real-time identification of large-space building fires and forecast of temperature development. Expert Systems with Applications, 255: 124758.

13. Junfeng C, Maohua Z, Peiyun Q, et al. (2023). Mapping the fire risk in buildings: A hybrid method of ASET-RSET concept and FED concept. Reliability Engineering & System Safety, 240: 109571.
14. Kebriyaee SA, Moghiman M, Niazmand H (2024). Empirical study on the influence of initial relative humidity on wood crib fire behavior in compartment under varied natural ventilation conditions. Fire Safety Journal, 148: 104229.
15. Khan AA, Zhang T, Huang X, et al. (2023). Machine learning driven smart fire safety design of false ceiling and emergency response. Process Safety and Environmental Protection, 177: 1294-1306.
16. Khan ZA, Hussain T, Ullah FUM, et al. (2022). Randomly Initialized CNN with Densely Connected Stacked Autoencoder for Efficient Fire Detection. Engineering Applications of Artificial Intelligence, 116: 105403.
17. Khanmohammadi S, Cruz MG, Perrakis DDB, et al. (2024). Using AutoML and generative AI to predict the type of wildfire propagation in Canadian conifer forests. Ecological Informatics, 82: 102711.
18. Kou L, Wang X, Guo X, et al. (2021). Deep learning based inverse model for building fire source location and intensity estimation. Fire Safety Journal, 121: 103310.
19. Lambert K, Merci B (2024). Analysis of air consumption and moving speed by firefighters during full-scale search & rescue experiments in a tunnel. Fire Safety Journal, 150: 104290.
20. LeCun Y, Bottou L, Bengio Y, et al. (1998). Gradient-based learning applied to document recognition. Proceedings of the IEEE, 86: 2278-2324.
21. Li C-Y, Zhang F, Chen L (2024). Robot-assisted pedestrian evacuation in fire scenarios based on deep reinforcement learning. Chinese Journal of Physics, 92: 494-531.
22. Li N, Huang G, Jiang H, et al. (2023). Fire propagation-driven dynamic intelligent evacuation model in multifloor hybrid buildings. Advanced Engineering Informatics, 57: 102097.
23. Liu G, Liu Z, Qu G, et al. (2024). Dual-agent intelligent fire detection method for large commercial spaces based on numerical databases and artificial intelligence. Process Safety and Environmental Protection, 191: 2485-2499.
24. Liu G, Meng H, Qu G, et al. (2023a). Distributed optical fiber sensor temperature dynamic correction method based on building fire temperature-time curve. Journal of Building Engineering, 68: 106050.
25. Liu G, Meng H, Qu G, et al. (2023b). Real-time monitoring and prediction method of commercial building fire temperature field based on distributed optical fiber sensor temperature measurement system. Journal of Building Engineering, 70: 106403.
26. Liu X, Xu Z-D, Sun B, et al. (2023c). Smart prediction for tunnel fire state evolution based on an improved fire simulation curve through particle swarm optimization algorithm. Fire Safety Journal, 136: 103763.
27. Liu Z, Lin J (2024). Combinatorial machine learning approaches for high-rise building cost prediction and their interpretability analysis. Journal of Asian Architecture and Building Engineering: 1-12.
28. Liu Z, Zhuang Y (2024). An investigation using resampling techniques and explainable machine learning to minimize fire losses in residential buildings. Journal of Building Engineering, 95: 110080.

29. Lyu H-F, Wang C-P, Deng J, et al. (2023). Human behaviour and evacuation time for large underground comprehensive buildings during fire risk process. Journal of Loss Prevention in the Process Industries, 84: 105134.
30. Majid S, Alenezi F, Masood S, et al. (2022). Attention based CNN model for fire detection and localization in real-world images. Expert Systems with Applications, 189: 116114.
31. McCracken T, Chen P, Metcalf A, et al. (2024). Quantifying the impacts of Canadian wildfires on regional air pollution networks. Science of The Total Environment, 928: 172461.
32. Moradi S, Hafezi M, Sheikhi A (2024). Early wildfire detection using different machine learning algorithms. Remote Sensing Applications: Society and Environment, 36: 101346.
33. NFRA C (2022). National Police and Fire situation in 2022. Available at: https://www.119.gov.cn/qmxfxw/xfyw/2023/36210.shtml.
34. Niu F, O'Neill Z, O'Neill C (2018). Data-driven based estimation of HVAC energy consumption using an improved Fourier series decomposition in buildings. Building Simulation, 11: 633-645.
35. Qu G, Zang X, Meng H, et al. (2023). A novel method for spatiotemporal temperature prediction in offices by using Raman-distributed fiber-optic sensor with the data fusion method. Journal of Building Engineering, 78: 107616.
36. Sangogboye FC, Arendt K, Singh A, et al. (2017). Performance comparison of occupancy count estimation and prediction with common versus dedicated sensors for building model predictive control. Building Simulation, 10: 829-843.
37. Shan X, Li Y, Jiang Y, et al. (2025). Experimental study and physical modeling of ceiling temperature distribution of fires in a large open-plan compartment with unilateral asymmetric openings. Case Studies in Thermal Engineering, 65: 105638.
38. Shen X, Cao Z, Liu H, et al. (2023). Inverse tracing of fire source in a single room based on CFD simulation and deep learning. Journal of Building Engineering, 76: 107069.
39. Sriniketh K, Le AV, Mohan RE, et al. (2023). Robot-aided human evacuation optimal path planning for fire drill in buildings. Journal of Building Engineering, 72: 106512.
40. Su P, Ding X-R, Zhang Y-T, et al. (2018). Long-term blood pressure prediction with deep recurrent neural networks. 2018 IEEE EMBS International conference on biomedical & health informatics (BHI). IEEE, 323-328.
41. Turska E, Jurga S, Piskorski J (2021). Mood disorder detection in adolescents by classification trees, random forests and XGBoost in presence of missing data. Entropy, 23: 1210.
42. Wang D, Ju X, Yang L (2023a). Experimental studies of the effect of burner location on the development of building fires. Journal of Building Engineering, 65: 105680.
43. Wang L, Lu H, Qu G, et al. (2024a). Cross-physical field prediction method for smoke field distribution in commercial building fire based on distributed optical fiber sensor. Journal of Building Engineering, 87: 109027.

44. Wang N, Xu Y, Wang S (2022). Interpretable boosting tree ensemble method for multisource building fire loss prediction. Reliability Engineering & System Safety, 225: 108587.
45. Wang Y, Yuan H, Wang J, et al. (2024b). Application of multi-objective artificial gorilla troops optimization algorithm in intelligent evacuation path planning for building fires. Journal of Building Engineering, 93: 109757.
46. Wang Y, Zhang Z, Wang Z, et al. (2024c). Interpretable Machine Learning-Based Text Classification Method for Construction Quality Defect Reports. Journal of Building Engineering: 109330.
47. Wang Z, Ding Y, Zhang T, et al. (2023b). Automatic real-time fire distance, size and power measurement driven by stereo camera and deep learning. Fire Safety Journal, 140: 103891.
48. Wang Z, Zhang T, Huang X (2023c). Predicting real-time fire heat release rate by flame images and deep learning. Proceedings of the Combustion Institute, 39: 4115-4123.
49. Wu C-H, Chen L-C (2012). 3D spatial information for fire-fighting search and rescue route analysis within buildings. Fire Safety Journal, 48: 21-29.
50. Wu X, Park Y, Li A, et al. (2021). Smart detection of fire source in tunnel based on the numerical database and artificial intelligence. Fire Technology, 57: 657-682.
51. Wu X, Zhang X, Huang X, et al. (2022). A real-time forecast of tunnel fire based on numerical database and artificial intelligence. Building Simulation. Springer, 1-14.
52. Zeng Y, Li Y, Du P, et al. (2023). Smart fire detection analysis in complex building floorplans powered by GAN. Journal of Building Engineering, 79: 107858.
53. Zhang L, Wu X, Liu M, et al. (2019). Discovering worst fire scenarios in subway stations: A simulation approach. Automation in Construction, 99: 183-196.
54. Zhang T, Ding F, Wang Z, et al. (2024a). Forecasting backdraft with multimodal method: Fusion of fire image and sensor data. Engineering Applications of Artificial Intelligence, 132: 107939.
55. Zhang T, Wang Z, Wong HY, et al. (2022a). Real-time forecast of compartment fire and flashover based on deep learning. Fire Safety Journal, 130: 103579.
56. Zhang X, Wu X, Huang X (2022b). Smart real-time forecast of transient tunnel fires by a dual-agent deep learning model. Tunnelling and Underground Space Technology, 129: 104631.
57. Zhang Y-Q, Wang J-H, Wang Y, et al. (2024b). Intelligent planning of fire evacuation routes in buildings based on improved adaptive ant colony algorithm. Computers & Industrial Engineering, 194: 110335.
58. Zhao J, Li W, Zhu J, et al. (2024). An efficient firefighting method for robotics: A novel convolution-based lightweight network model guided by contextual features with dual attention. Computers in Industry, 161: 104127.
59. Zhu Z, Zhou M, Hu F, et al. (2024). TSILNet: A novel hybrid model for energy disaggregation based on two-stage improved TCN combined with IECA-LSTM. Building Simulation, 17: 2083-2095.

Figures

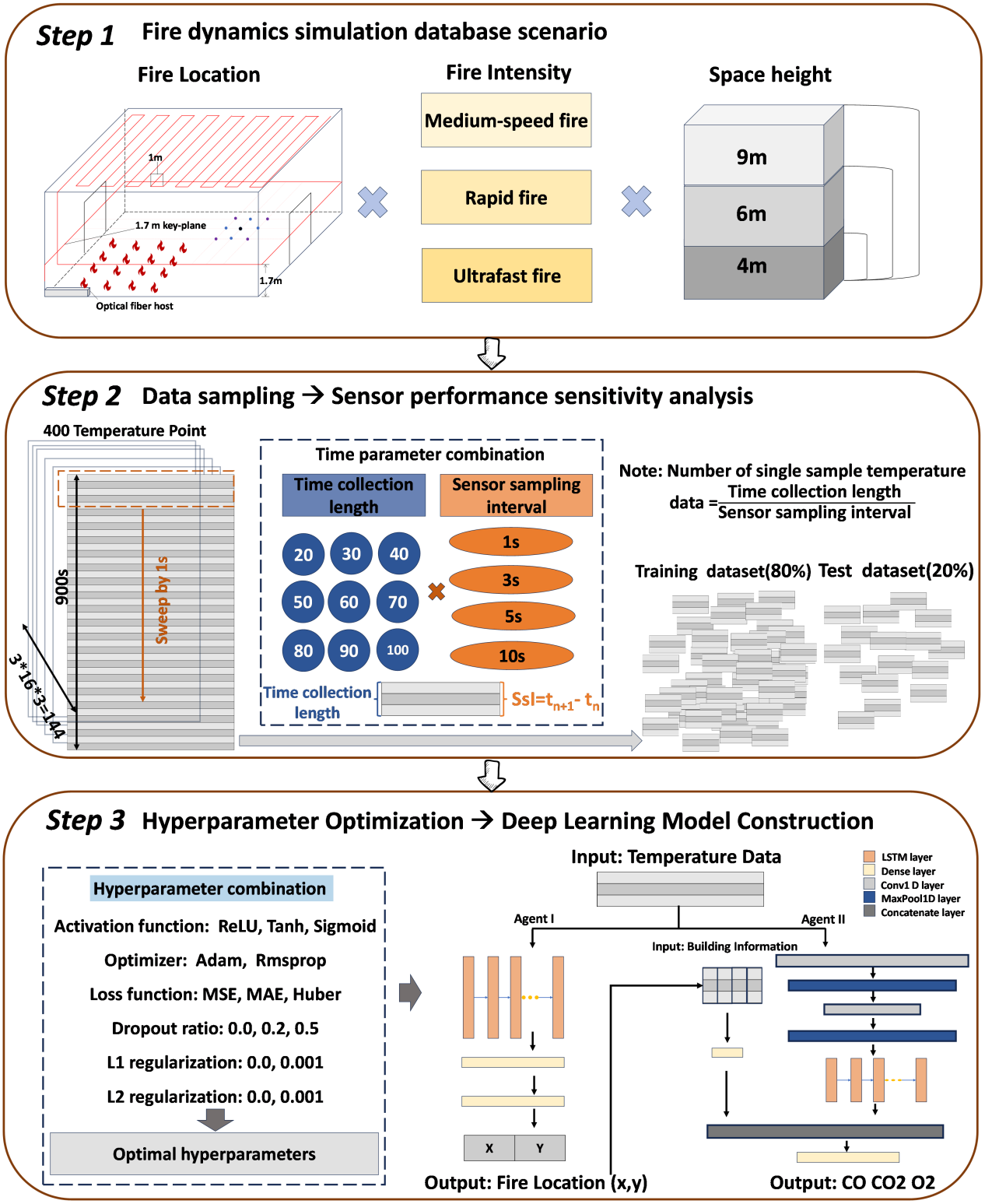


Figure 1

Research framework

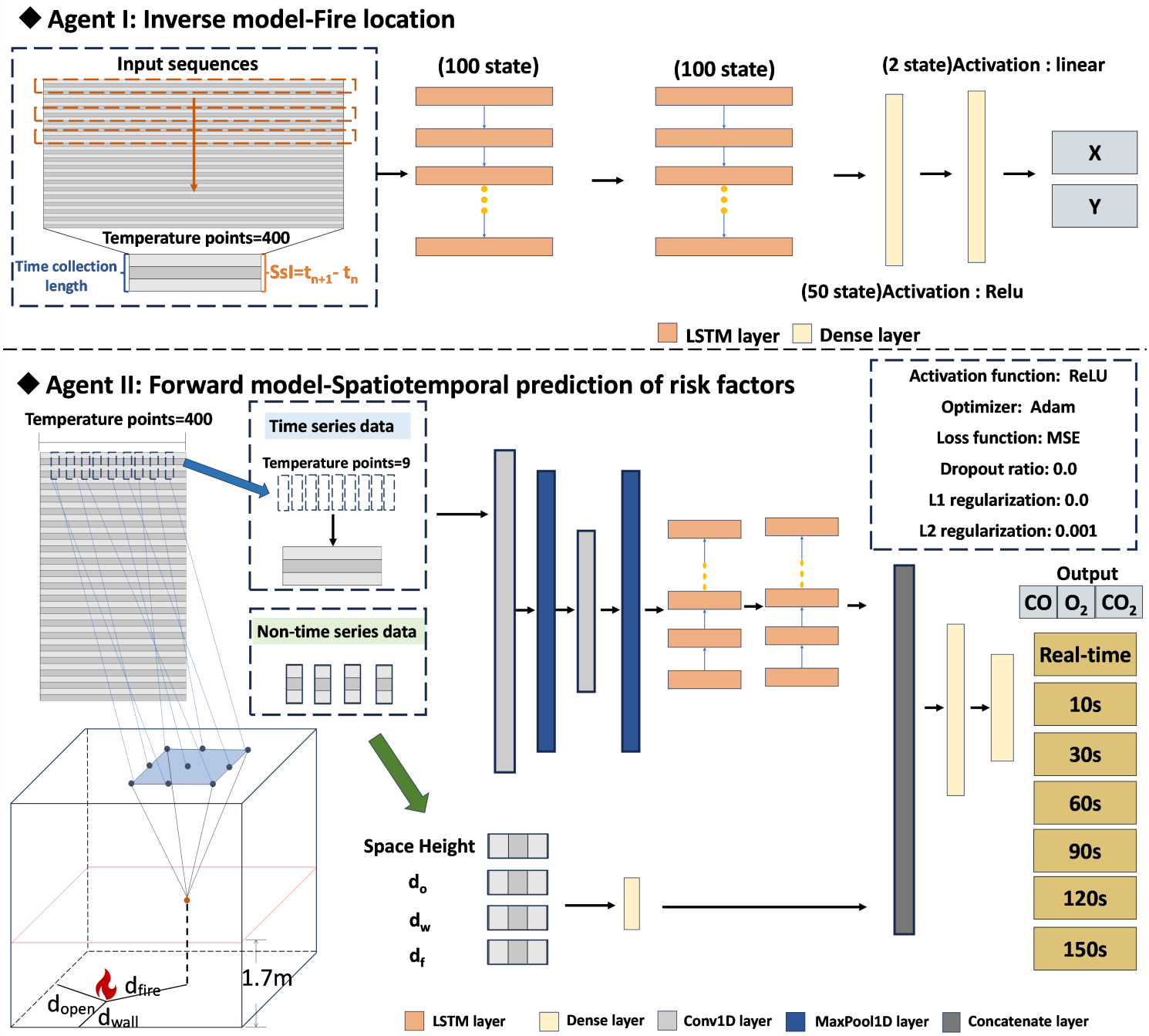


Figure 2

Model structure and details

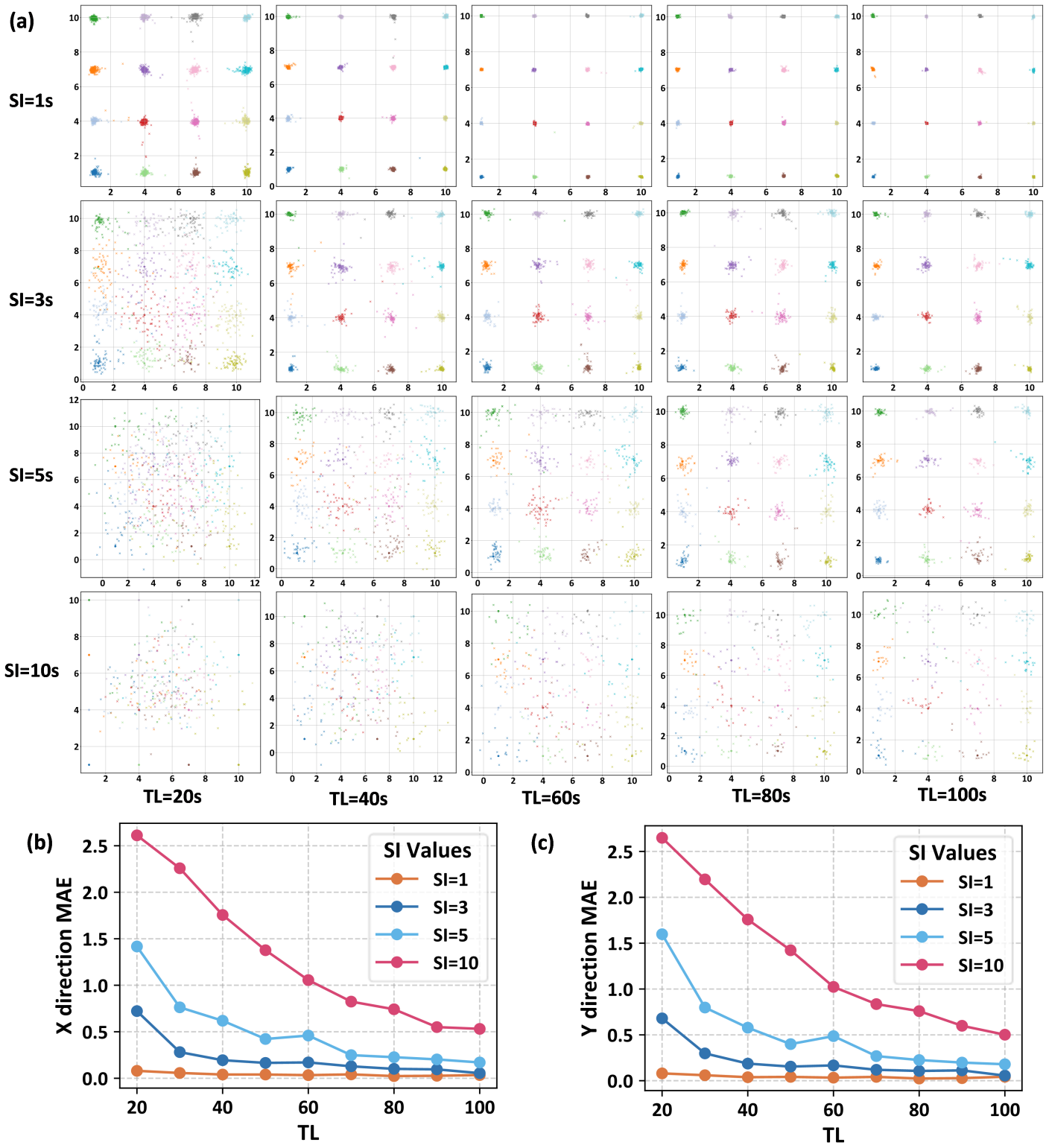


Figure 3

Position and Prediction Model Results(a) Position Recognition Plan Display(b) MAE in the x-direction as a function of TL(c) MAE in the y-direction as a function of TL

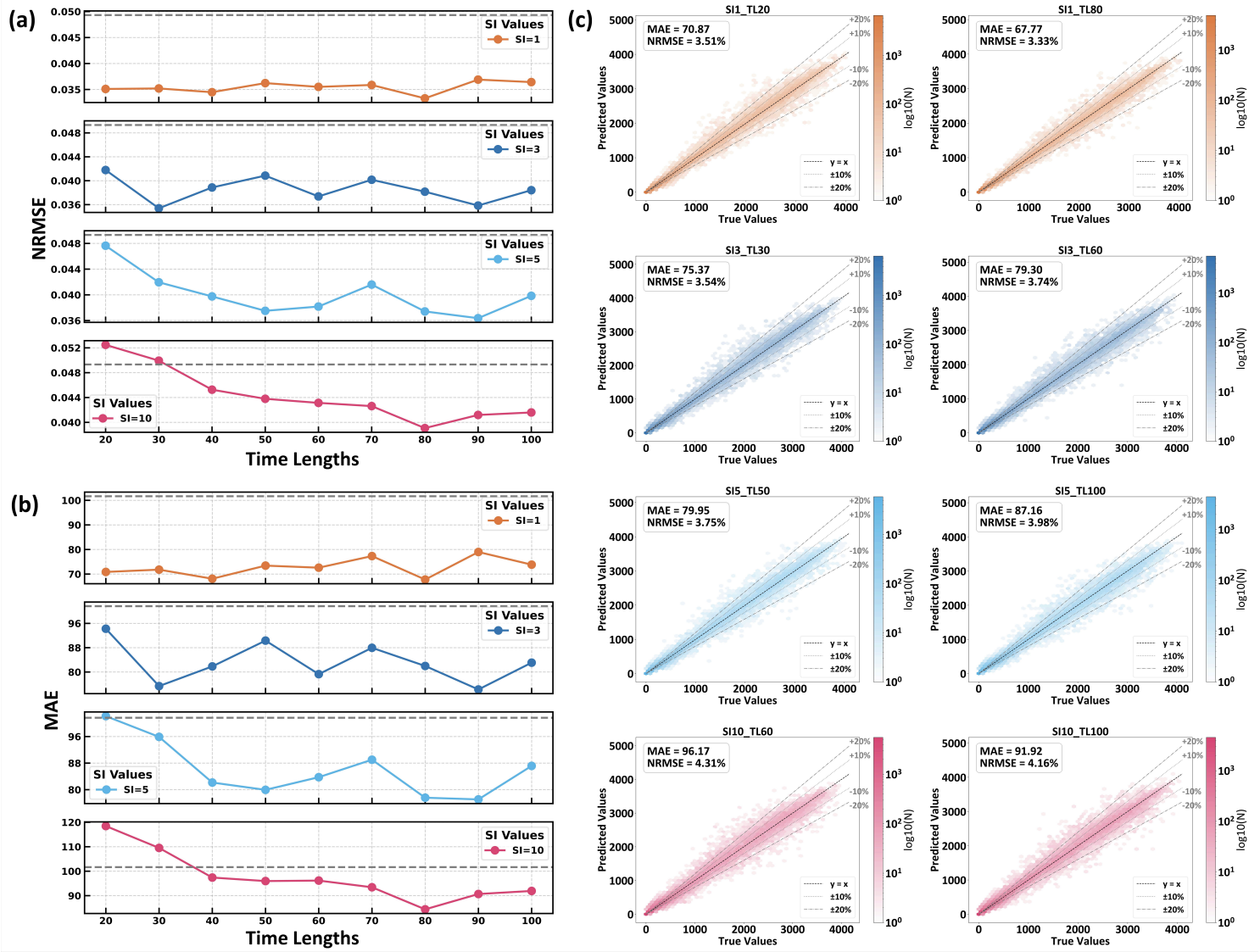


Figure 4

shows the results of the CO real-time monitoring model: (a) NRMSE as it changes with TL under four different SI conditions, (b) MAE as it changes with TL under four different SI conditions, and (c) the comparison between the true values and predicted values for eight cases.

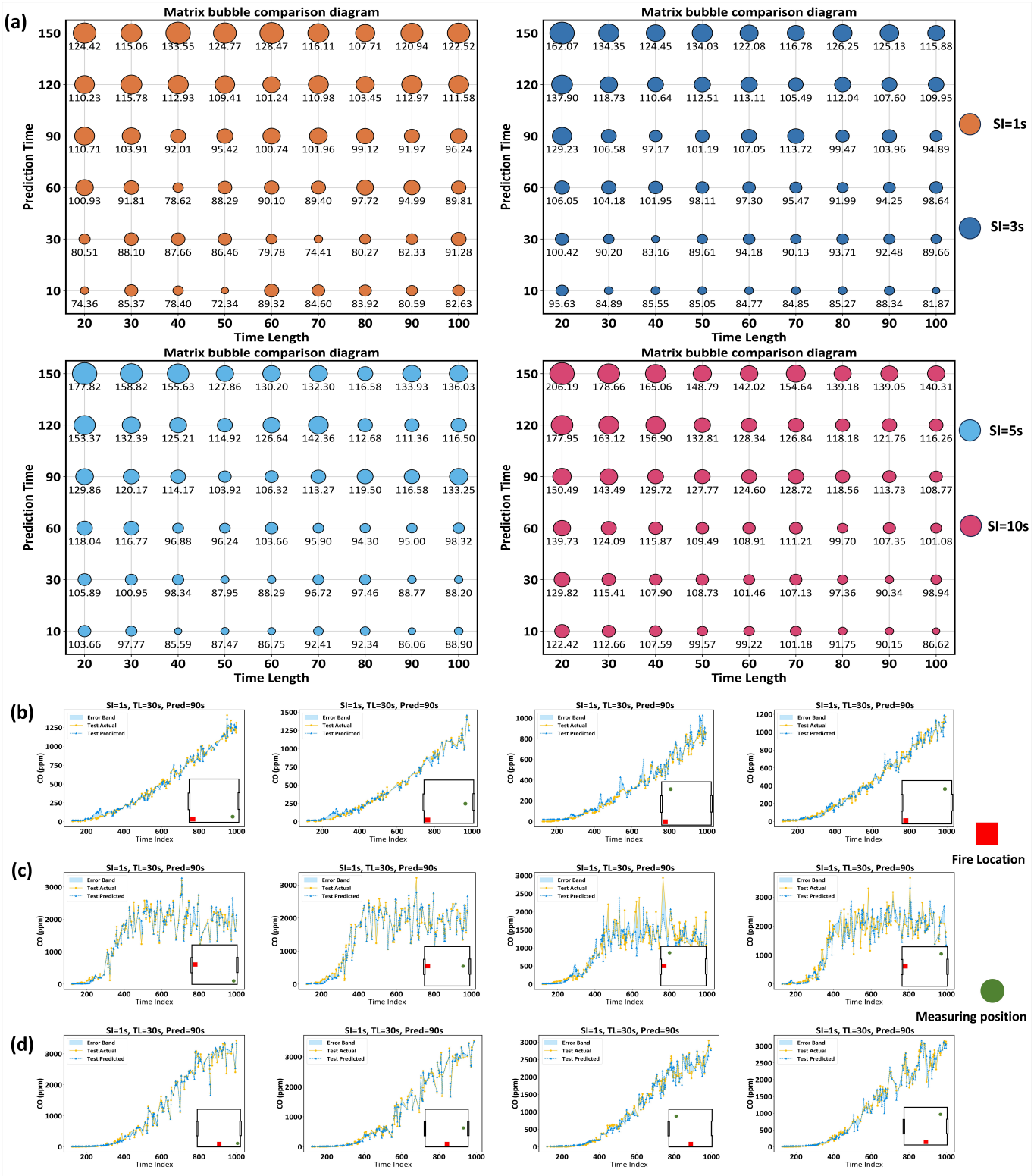


Figure 5

shows the results of the CO advanced monitoring model: (a) MAE as it changes with TL and PT under four different SI conditions, (b) comparison of predictions for four representative measurement points in a medium-speed fire scenario with a source location at (1m, 1m) and a height of 4m, (c) comparison of predictions for four representative measurement points in a fast fire scenario with a source location at

(1m, 10m) and a height of 6m, and (d) comparison of predictions for four representative measurement points in an ultra-fast fire scenario with a source location at (10m, 1m) and a height of 9m.

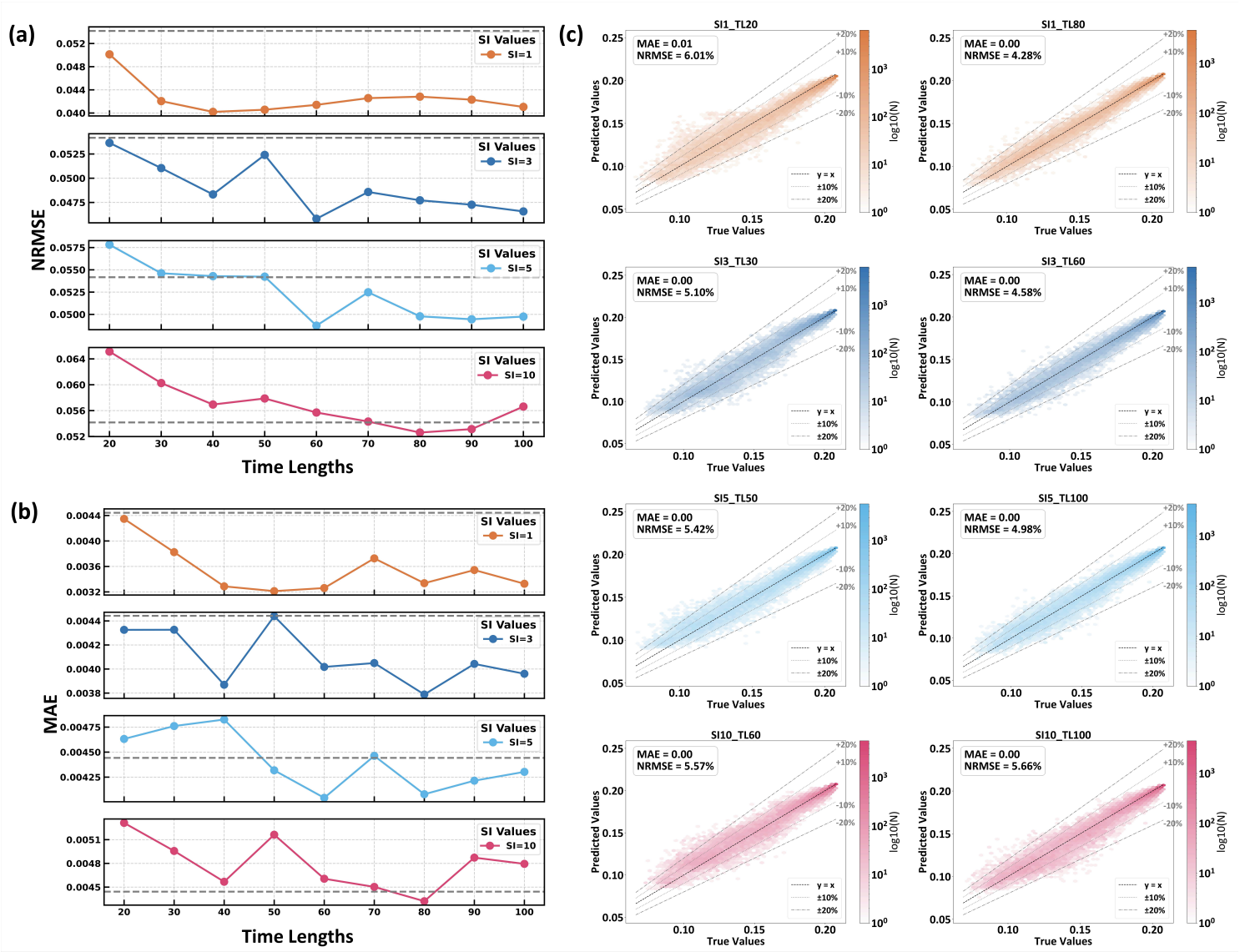


Figure 6

shows the results of the O_2 real-time monitoring model: (a) NRMSE as it changes with TL under four different SI conditions, (b) MAE as it changes with TL under four different SI conditions, and (c) the comparison between the true values and predicted values for eight cases.

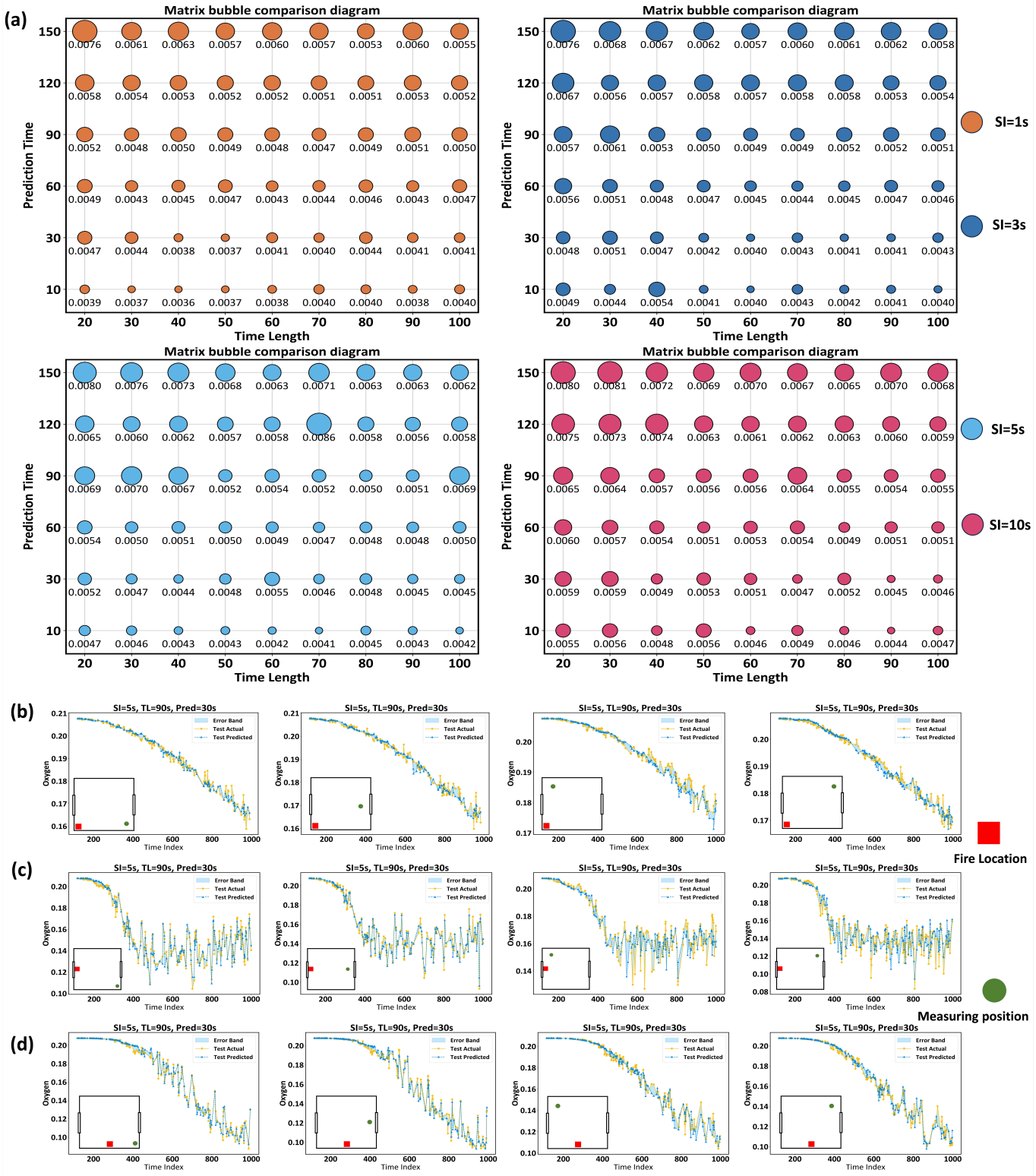


Figure 7

shows the results of the O_2 advanced monitoring model: (a) MAE as it changes with TL and PT under four different SI conditions, (b) comparison of predictions for four representative measurement points in a medium-speed fire scenario with a source location at (1m, 1m) and a height of 4m, (c) comparison of predictions for four representative measurement points in a fast fire scenario with a source location at

(1m, 10m) and a height of 6m, and (d) comparison of predictions for four representative measurement points in an ultra-fast fire scenario with a source location at (10m, 1m) and a height of 9m.

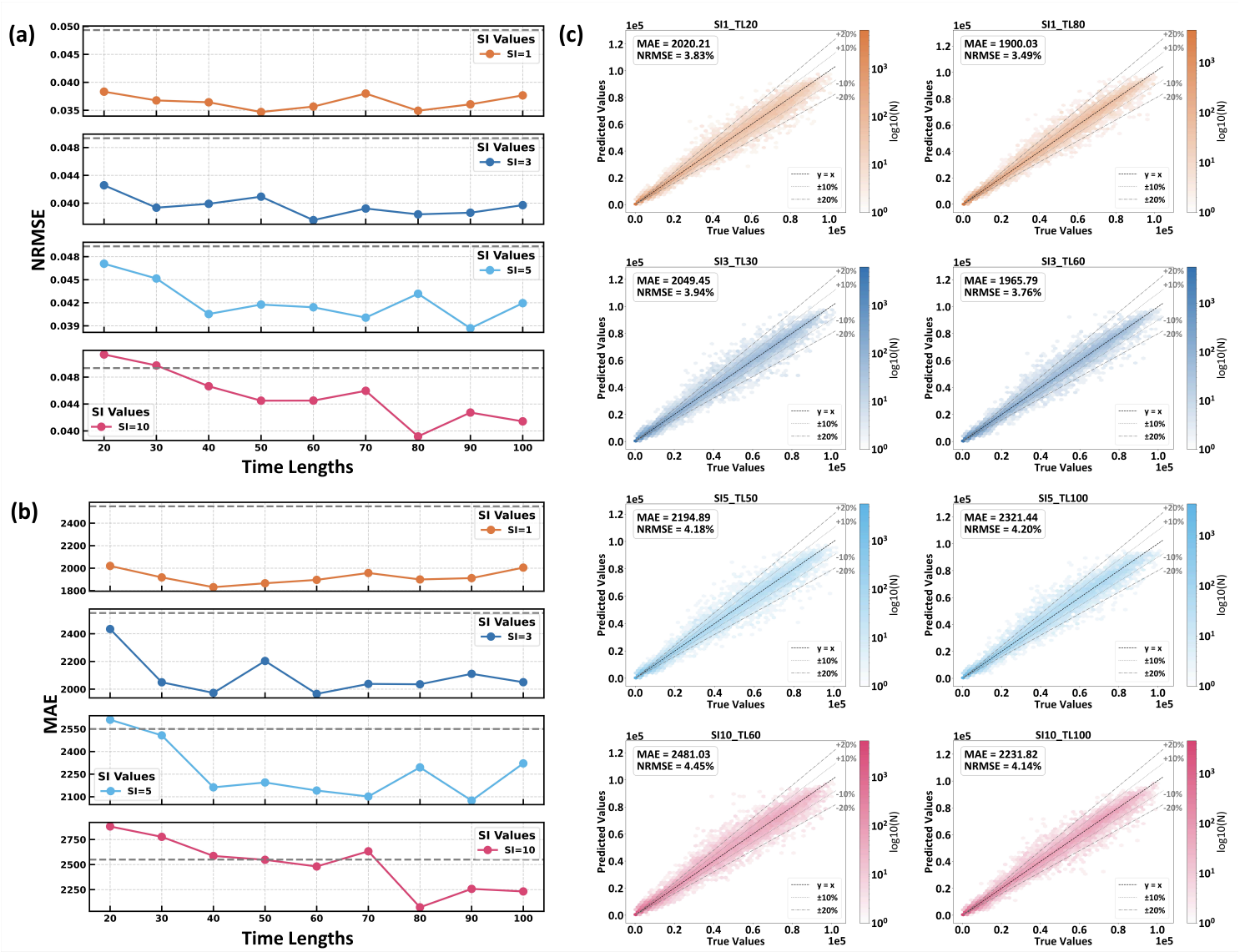


Figure 8

shows the results of the CO_2 real-time monitoring model: (a) NRMSE as it changes with TL under four different SI conditions, (b) MAE as it changes with TL under four different SI conditions, and (c) the comparison between the true values and predicted values for eight cases.

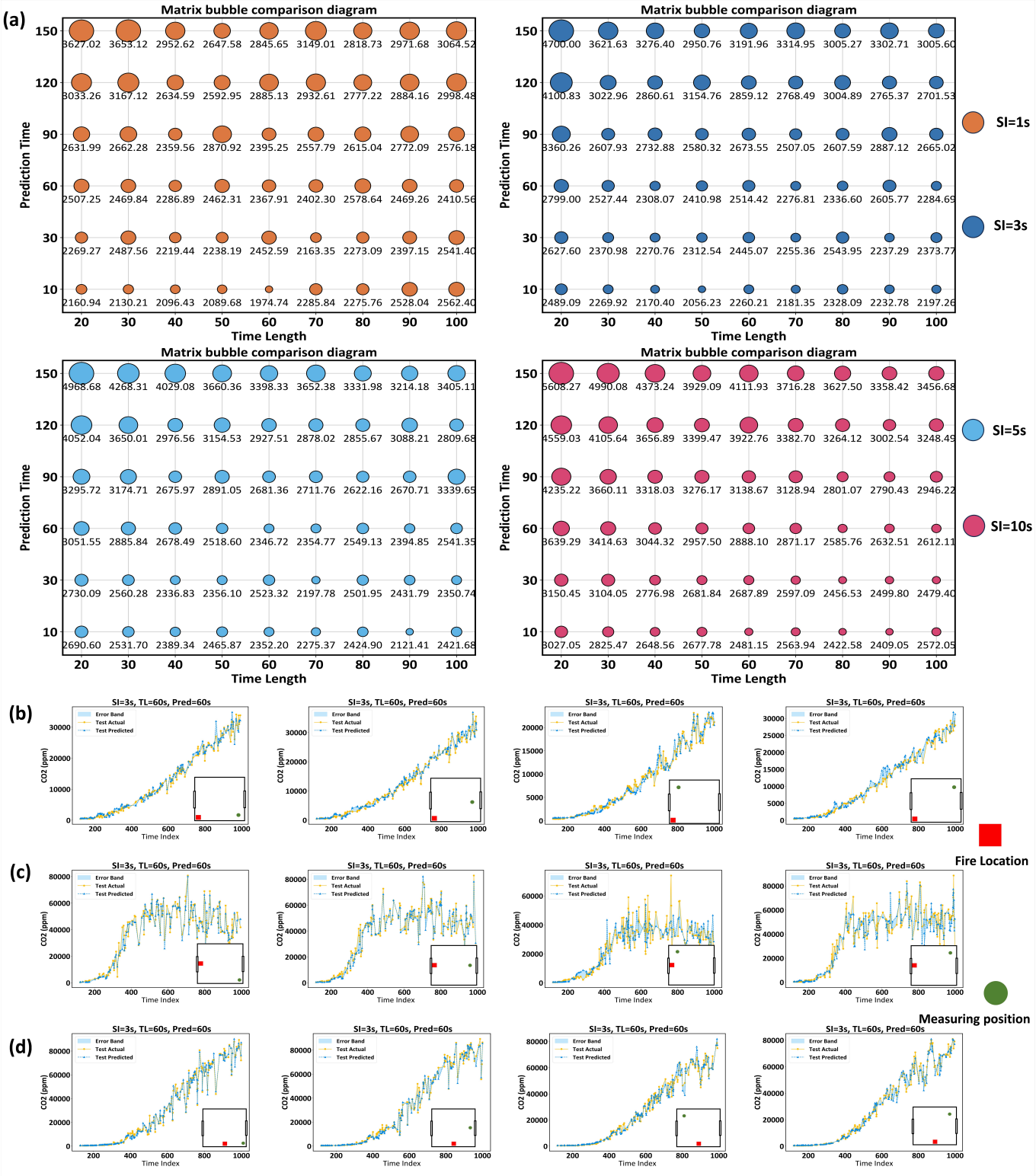


Figure 9

shows the results of the CO_2 advanced monitoring model: (a) MAE as it changes with TL and PT under four different SI conditions, (b) comparison of predictions for four representative measurement points in a medium-speed fire scenario with a source location at (1m, 1m) and a height of 4m, (c) comparison of predictions for four representative measurement points in a fast fire scenario with a source location at

(1m, 10m) and a height of 6m, and (d) comparison of predictions for four representative measurement points in an ultra-fast fire scenario with a source location at (10m, 1m) and a height of 9m.

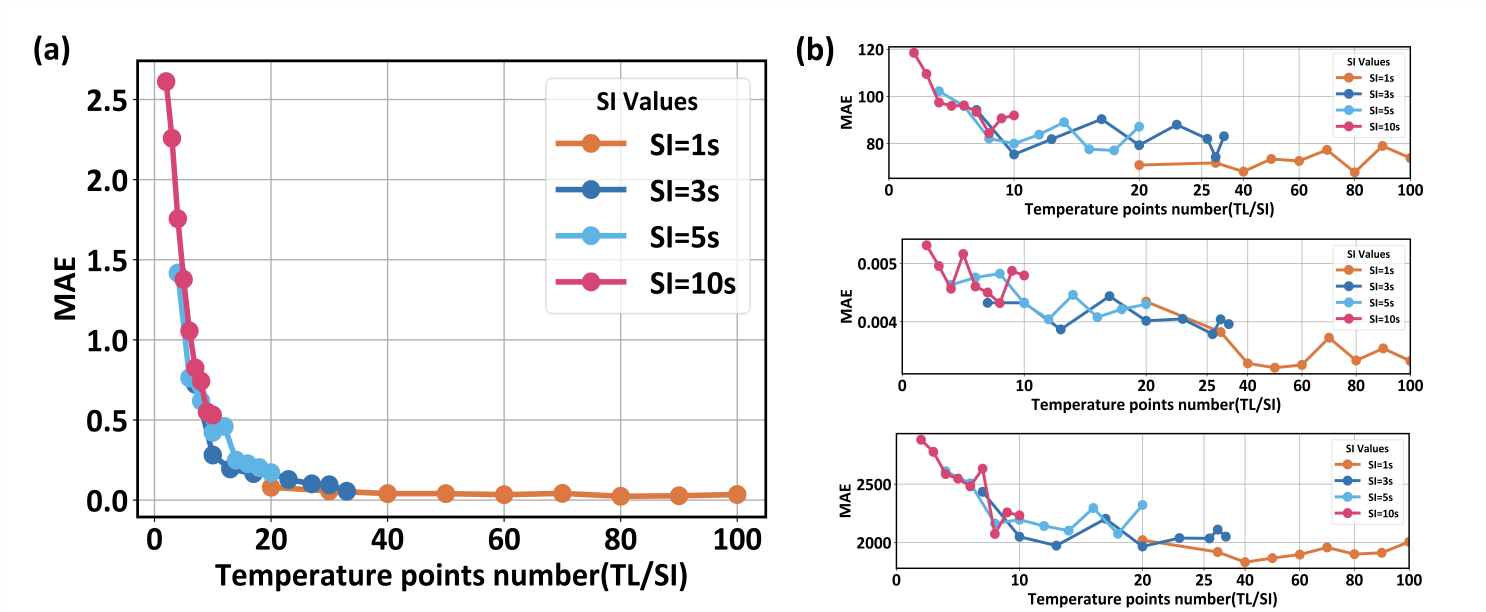


Figure 10

shows the change in model performance with the number of temperature points: (a) Location prediction model, (b) Hazard factor spatiotemporal prediction model.

Supplementary Files

This is a list of supplementary files associated with this preprint. Click to download.

- Appendix.docx